Chinese Journal of Structural Chemistry

ARTICLE

$Ni(OH)_2$ Derived from NiS_2 Induced by Reflux Playing Three Roles for Hydrogen/Oxygen Evolution Reaction

Sheng-Jun Xu[1]*, Ya-Nan Zhou[2], Guo-Ping Shen[2] and Bin Dong[2]*

[1]*Dongying Haike Ruilin Chemical Co., LTD., Dongying 257000, China*

[2]*State Key Laboratory of Heavy Oil Processing, College of Chemistry and Chemical Engineering, China University of Petroleum (East China), Qingdao 266580, China*

ABSTRACT Developing efficient and promising non-noble catalysts for oxygen evolution reaction (OER) and hydrogen evolution reaction (HER) is vital but still a huge challenge for the clean energy system. Herein, we have integrated the active components for OER ($Ni(OH)_2$) and HER (NiS_2 and $Ni(OH)_2$) into $Ni(OH)_2$@NiS_2 heterostructures by a facile reflux method. The in-situ formed $Ni(OH)_2$ thin layer is coated on the surface of hollow NiS_2 nanosphere. The uniform $Ni(OH)_2$@NiS_2 hollow sphere processes enlarge the electrochemically active specific surface area and enhance the intrinsic activity compared to NiS_2 precursor, which affords a current density of 10 mA cm^{-2} at the overpotential of 309 mV and 100 mA cm^{-2} at 359 mV for OER. Meanwhile, $Ni(OH)_2$@NiS_2 can reach 10 mA cm^{-2} at 233 mV for HER, superior to pure NiS_2. The enhanced performance can be attributed to the synergy between $Ni(OH)_2$ and NiS_2. Specifically, $Ni(OH)_2$ has three functions for water splitting: providing active sites for hydrogen adsorption and hydroxyl group desorption and working as real OER active sites. Moreover, $Ni(OH)_2$@NiS_2 displays great stability for OER (50 h) and HER (30 h).

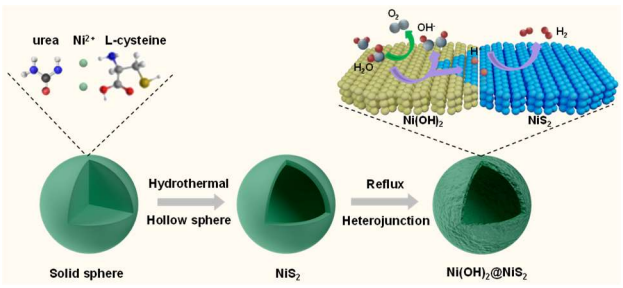

Keywords: $Ni(OH)_2$, NiS_2, heterostructures, oxygen evolution reaction, hydrogen evolution reaction

■ INTRODUCTION

The increasingly petrochemical energy crises and environmental pollution concerns have aroused enormous concerns for the sustainable development of human society. In this background, the electricity derived from renewable energy such as wind and solar energy draws much attention.[1-3] Considering the diurnal and seasonal variations of wind and solar, it may be more fascinating to store them in the form of carbon-free fuel for later use. Therefore, the development of high-effective and economic electrocatalysts for water splitting including oxygen evolution reaction (OER) and hydrogen evolution reaction (HER) is crucial to bridge the gap between green energy systems and energy storage technology.[4-6] Nobel metal materials, such as Ru/Ir- and Pt-based materials, are deemed as the most state-of-the-art electrocatalysts and are used as the benchmarks.[7,8] Nevertheless, the high cost and severe scarcity have gravely limited their industrial application. The earth-abundant materials like chalcogenides,[9,10] borides,[11,12] carbides[13,14] and hydroxides[15,16] alternative to noble metal-based catalysts are popular research hotspots for electrocatalytic water splitting.

No matter for HER or OER in alkaline electrolytes, the sluggish kinetics is needed to be overcome. Specifically, for OER, the comment four proton-coupled electron-transfer process restricts the total efficiency of hydrogen production.[17-19] The hydroxides have been reported as one of the most effective catalysts for OER because of their appropriate absorption for oxygen intermediate.[20-22] When it comes to HER, an extra water molecule dissociation step must be taken into account.[23,24] In this regard, a water cleavage "promoter" has been tried, among which, the hydroxides are the great one thanks to good water affinity.[25,26] As such, the integration of hydroxides and other active compounds is expected to be a resultful strategy to boost OER and HER performance in alkaline media. Some proven examples consist of WN-$Ni(OH)_2$,[27] $Ni(OH)_2$-Pt,[28] $Ni(OH)_2/Ni_3S_2$[29] and so forth. In addition, the alkaline HER includes the extra water adsorption step, water dissociation step and OH_{ad} desorption step.[30,31] It would be better for water splitting if the water adsorption and OH_{ad} desorption can be boosted simultaneously. Over the past few years, transition-metal dichalcogenides have been poured into many attractions due to the fast electron transport and favorable lifetime.[32-34] Among them, NiS_2 has been widely reported as a useful HER catalyst.[32,33] Moreover, sulfides with heterostructure show higher catalytic activity via enhanced coupling and charge transfer.[33] Fan et al. synthesized the bimetallic sulfides MoS_2-NiS_2 anchored three-dimensional nitrogen-doped graphene foam hybrid for efficient overall water splitting.[33] Besides, the hollow can endow the catalyst with a larger active surface area and thus provide sufficient attachment for active components.[34] Therefore, the integration of hydroxides with hollow NiS_2 can further elevate catalytic performance for OER and HER and it deserves deeper research.

Herein, we have designed a heterostructured $Ni(OH)_2$@NiS_2 catalyst by a sample hydrothermal reaction followed by a mild reflux process. Here, the $Ni(OH)_2$ displays three functions, working as an effective OER material, providing the active center for hydrogen adsorption during water dissociation, and meanwhile promoting OH_{ad} desorption. As a result, the final $Ni(OH)_2$@NiS_2 shows enhanced catalytic activity for both OER and HER com-

DOI: 10.14102/j.cnki.0254-5861.2022-0143

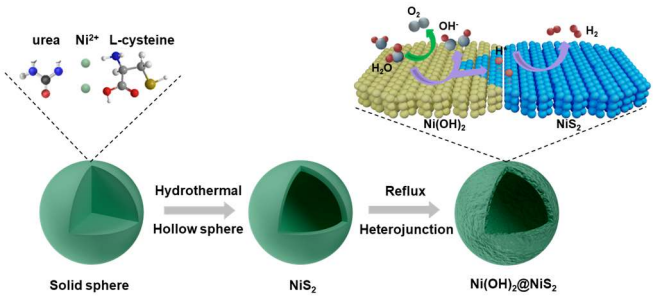

Figure 1. Schematic illustration of the formation of $Ni(OH)_2@NiS_2$ hollow spheres.

pared with pure NiS_2 without $Ni(OH)_2$ loading in 1.0 M KOH. The $Ni(OH)_2@NiS_2$ hybrid only requires 309 and 359 mV at 10 and 100 mA cm^{-2} with a lifetime of 50 h (10 mA cm^{-2}) towards OER. Besides, the composite also works well in the HER with the overpotential at 10 mA cm^{-2} dropped by 65 mV compared with the NiS_2 precursor. Our work is expected to provide a deeper insight into the design of high-performance electrocatalysts for water splitting by interface modification.

RESULTS AND DISCUSSION

Figure 1 illustrates the synthetic procedure of $Ni(OH)_2@NiS_2$ hollow spheres. Firstly, the NiS_2 was synthesized by a sample hydrothermal reaction with the L-cysteine as the assembly template agent and sulfide source. In detail, L-cysteine is featured with multiple functional groups including $-COO^-$, -SH and $-NH_2$, which tend to coordinate with nickel ions to form Ni^{2+}-L-cysteine intermediate.[35] When heated, L-cysteine can release H_2S as the sulfide source to finally produce NiS_2. At the initial phase of the reaction, the NiS_2 shows a strong tendency to aggregate into solid spherical products in view of the minimization of the interfacial energy, as shown in Figure S1.[36] As the reaction time lengthens, the Ni-coordinated compound dissociated from inside with the organic residues transferred to the internal space, thus generating the core-shell structured NiS_2 sphere on the basis of the Ostwald ripening effect.[37] Subsequently, during the reflux process in the mixed solvent of deionized water and ethanol, the OH^- ions released from the solution at 85 ℃ would gradually consume Ni^{2+} ions of NiS_2 to generate a $Ni(OH)_2$ thin layer on the surface of NiS_2.

The morphological features of the obtained samples were characterized by scanning electron microscopy (SEM). In Figure 2a-b, NiS_2 shows the uniform hollow sphere structure with diameters of

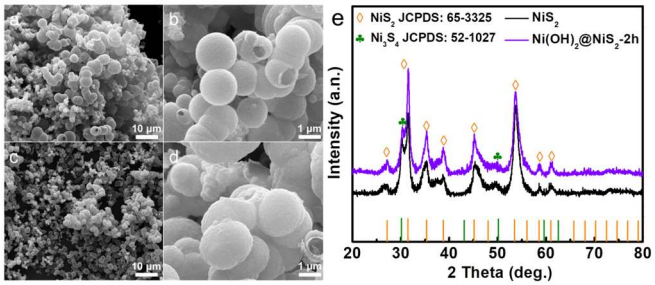

Figure 2. SEM images of (a, b) NiS_2 precursor and (c, d) $Ni(OH)_2@NiS_2$-2h. (e) XRD of NiS_2 and $Ni(OH)_2@NiS_2$-2h samples.

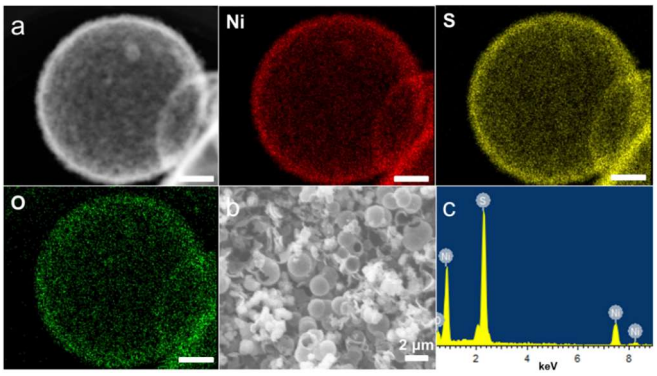

Figure 3. (a) Element mappings of $Ni(OH)_2@NiS_2$-2h. Scale bar: 200 nm. (b) SEM image of $Ni(OH)_2@NiS_2$-2h and corresponding EDX characterization.

around 2 μm, as proved by some broken ones. After refluxing, $Ni(OH)_2@NiS_2$ maintains the sphere structure well and displays a more rough surface due to the formation of $Ni(OH)_2$ on the surface (Figure 2c-d), which implies more surface areas and active sites for catalytic water splitting, as Figure S2 confirms. Besides, with the increase of reflux time, the $Ni(OH)_2$ layer becomes noticeably thicker (Figure S3). X-ray diffraction (XRD) was further collected to characterize the crystal structure and composition. As shown in Figure 2e, in addition to the peaks at 30.4 and 50.0° attributed to Ni_3S_4, the XRD pattern of the NiS_2 precursor is matched well with the cubic NiS_2 (JCPDS: 65-3325, space group: Pa-3, a = b = c = 5.678 Å). After subsequent reflux, the XRD pattern shows no obvious changes, possibly because the reflux does not destroy the crystal structure of NiS_2. Meanwhile, the newly formed $Ni(OH)_2$ layer is in trace amounts and homogeneously disperses on the surface of NiS_2. Nevertheless, it can be easily discerned that the XRD peaks of final $Ni(OH)_2@NiS_2$ shift to a higher degree compared with that of initial NiS_2, demonstrating that $Ni(OH)_2$ and NiS_2 have been integrated closely and induced lattice distortion at the interface. Moreover, this shift also suggests decreased lattice distance of $Ni(OH)_2@NiS_2$ sample due to the fact that the S atoms with larger atomic radius have been partially substituted by the O atoms. In addition, the $Ni(OH)_2$ signals can also be decerned (JCPDS: 06-0044), which overlaps with the standard NiS_2 peaks (Figure S4), signifying the successful synthesis of $Ni(OH)_2$ layer.

Furthermore, the hollow sphere was also testified by the high angle ring dark field image-scanning transmission electron microscope (HAADF-STEM) in Figure 3a, from which the shell thickness is identified to be 40-50 nm. The related element mapping demonstrates the uniform distribution of Ni, S and O elements in $Ni(OH)_2@NiS_2$. Additionally, energy dispersive X-ray (EDX) in the selected area (Figure 3b) determines the atomic ratio of Ni:S:O to be 1:1.5:1.1 (Figure 3c).

Further, we detected the chemical component and valence state near the surface of NiS_2 and $Ni(OH)_2@NiS_2$ samples by X-ray photoelectron spectroscopy (XPS). For the NiS_2 sample, the peaks located at 855.6 and 873.4 eV can be ascribed to the Ni $2p_{3/2}$ and Ni $2p_{1/2}$ (Figure 4a), respectively, suggesting the successful synthesis of the NiS_2 precursor.[36,38,39] For $Ni(OH)_2@NiS_2$ catalyst, a pair of new peaks at 857.32 and 876.33 eV can be

DOI: 10.14102/j.cnki.0254-5861.2022-0143

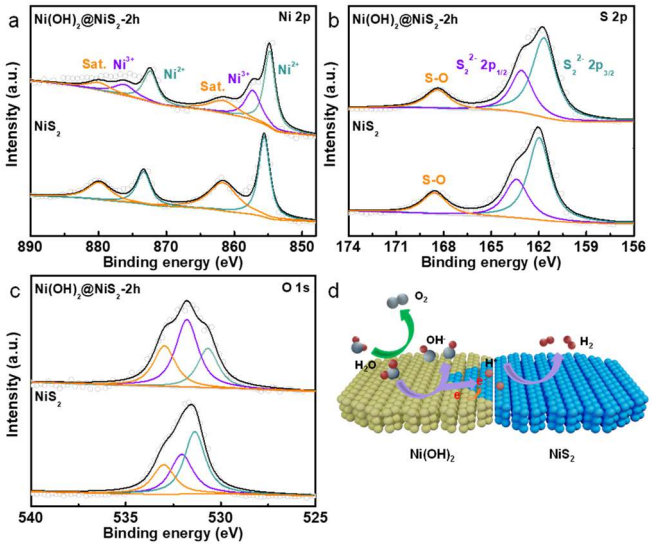

Figure 4. (a) Ni 2p, (b) S 2p and (c) O 1s of NiS_2 and $Ni(OH)_2@NiS_2$ samples. (d) Illustration of charge transfer and HER process

deconvoluted, corresponding to the Ni^{3+} species.[40] In the S 2p region (Figure 4b), the peak at 168.4 eV comes from the S-O species, while the S_2^{2-} $2p_{3/2}$ and S_2^{2-} $2p_{1/2}$ can be found at 161.7 and 163.1 eV.[41] Compared with the NiS_2 sample, the S 2p XPS of $Ni(OH)_2@NiS_2$ moves to lower binding energy, indicating the strong electron interaction between the heterostructure interface. For O 1*s* XPS (Figure 4c), the fitted three peaks at 530.7, 531.8 and 533.0 eV are related to the lattice oxygen, defective oxygen and adsorbed oxygen on the surface of the catalyst.[42,43] It is clear that the content of defective oxygen shows an obvious rise for $Ni(OH)_2@NiS_2$, which means that reflux treatment can induce more defects, as Figure S5 shows. According to Wang,[44] the oxygen defects can induce the surface reconstruction by triggering the pre-oxidation of metal sites at a relatively low potential. Besides, it has been verified that the oxygen defects facilitate the adsorption of OH^- and lower the energy for the formation of adsorbed oxygen on the surface of the catalyst.[45] All of the above results suggest the successful preparation of hollow structured $Ni(OH)_2@NiS_2$ with a heterostructure $Ni(OH)_2$ and NiS_2 interface. Semiconductor physics has pinpointed that the heterojunction system with two semiconductors with different energy structures can lead to the generation of a built-in electric field, which can accelerate electron transfer in electrocatalytic processes and affect the adsorption of active reactants.[46,47]

To validate the important role of $Ni(OH)_2$ in electrocatalytic water splitting, we constructed a typical three-electrode configuration in 1.0 M KOH to research the catalytic performance of all synthesized samples. For comparison, commercial RuO_2 and Pt/C (20 wt% Pt) electrodes prepared under the same condition were used as the benchmarks for OER and HER.

At first, we measured the OER activity of NiS_2 and $Ni(OH)_2@NiS_2$ with different reflux times, and the linear sweep voltammetry (LSV) polarization curves are plotted in Figure 5a. The NiS_2 precursor displays a better OER activity than RuO_2, requiring the overpotentials of 362 mV at 10 mA cm^{-2}. After reflux treatment, the water

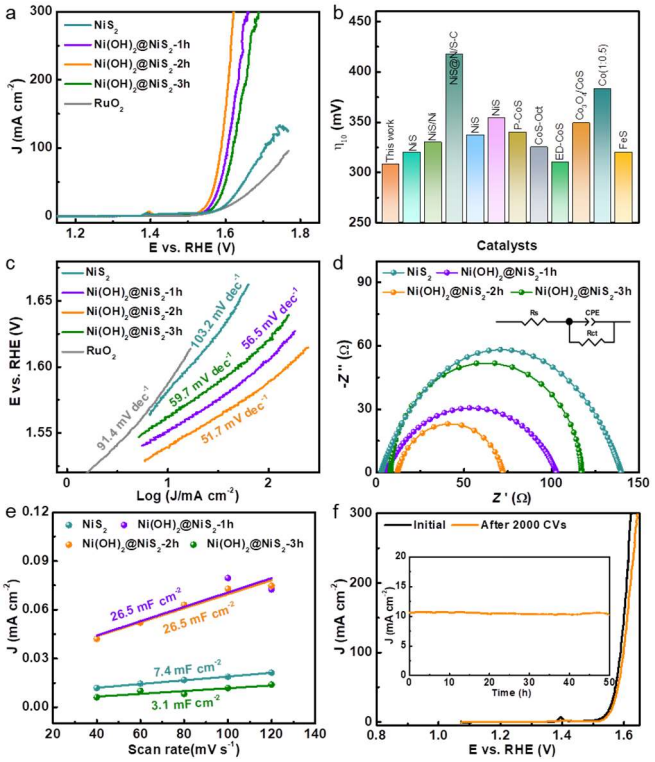

Figure 5. (a) LSV curves of all synthesized samples. (b) Comparison of overpotential at 10 mA cm^{-2} for sulfide catalysts in Table S1. (c) Tafel slopes, (d) EIS and (e) C_{dl} plots of obtained samples. (f) LSV plots of $Ni(OH)_2@NiS_2$-2h before and after 2000 CVs. The insert is the *i-t* curves at 1.56 V vs. RHE.

oxidation performance shows a great improvement, of which the $Ni(OH)_2@NiS_2$-2h exhibits the best catalytic activity with the overpotentials of 309 and 359 mV to deliver 10 and 100 mA cm^{-2}, which is also superior to the previously reported catalysts (Figure 5b, Table S1). The OER activity for $Ni(OH)_2@NiS_2$-2h reaches the best, suggesting that the appropriate $Ni(OH)_2$ is conductive to OER because of the accelerated formation and the electrophilic properties of adsorbed oxygenated species on the activated Ni sites. With further increase of $Ni(OH)_2$, the heterogeneous interfaces are covered and cannot be exposed, resulting in inferior OER performance. We supposed that the small difference in OER activity for samples at different reflux time may result from the limited formation of $Ni(OH)_2$ after 1h, since $Ni(OH)_2$ was generated through the dissolution of Ni^{2+} from NiS_2. The newly produced $Ni(OH)_2$ may hinder the contact of Ni^{2+} with the leached OH^- ions, in turn, slowing the formation of $Ni(OH)_2$.

Further, Tafel slopes were calculated from respective LSV curves to discover the catalytic kinetics. As Figure 5c manifests, the Tafel slope of $Ni(OH)_2@NiS_2$-2h is 51.7 mV dec^{-1}, much lower than the fresh NiS_2 (103.2 mV dec^{-1}). Such result suggests that the oxygen evolution electrocatalysis is determined by the association of OH reactants on active sites.[48] Furthermore, electrochemical impedance spectroscopy (EIS) was conducted to gain more information about the electron transfer kinetics. The used equivalent circuit is shown in the illustration of Figure 5d, where

DOI: 10.14102/j.cnki.0254-5861.2022-0143

the R_s, R_{ct} and CPE represent the internal resistance of electrolyte and electrode, charge transfer resistance and constant phase angle element, respectively. $Ni(OH)_2$@NiS_2-2h owns smaller R_{ct} value (60.4 Ω) than NiS_2 (137.5 Ω) and other control samples, indicating that the charge exchange has been expedited thanks to the high intrinsic electrical conductivity of $Ni(OH)_2$-NiS_2 interface.[49]

To acquire the origin of OER activity for $Ni(OH)_2$@NiS_2-2h, the ECSA was further evaluated by means of a series of CV curves (Figure S6). In view of the linear relationship between ECSA and the double-layer capacitance (C_{dl}), we assessed the C_{dl} values of all samples (Figure 5e). The C_{dl} of $Ni(OH)_2$@NiS_2-2h is 26.5 mF cm^{-2}, which is around 3.6-fold higher than that if pure NiS_2 (7.4 mF cm^{-2}) is attributed to the rougher surface and sphere structure, increasing the specific surface area of active compounds. This reveals that the enlarged active area plays a significant role in boosting the OER activity. Stability is another critical parameter for electrocatalysts in addition to activity, thus the fast CV scan was implemented using the best-performed $Ni(OH)_2$@NiS_2-2h as the research object. The LSV curves before and after 2000 CVs are plotted in Figure 5f, showing only a decrease of 9 mV at 10 mA cm^{-2}. Besides, the long-term stability was also measured at the constant potential of 1.56 V vs. RHE. The stable *i-t* curve and well-maintained special structure disclose the favorable durability of $Ni(OH)_2$@NiS_2-2h (Figure 5f, Figure S7a), better than commercial RuO_2 (Figure S8a). Furthermore, XRD shows dispersed peaks (Figure S7c), suggesting the evolution of $Ni(OH)_2$@NiS_2-2h from well-crystallized $Ni(OH)_2$ and NiS_2 to amorphous nickel oxyhydroxides during water oxidation. We then analyzed the changes in the electronic structure of $Ni(OH)_2$@NiS_2-2h. As Figure S7d displays, the content of Ni^{3+} species is obviously increased. Besides, the Ni 2p peaks after OER shift to higher binding energy, identifying the formation of higher-valence Ni components. The movement of O 1s and S 2p peaks is possibly due to the interaction between the O and S atoms with the newly produced high-valence Ni atom (Figure S7e-f).

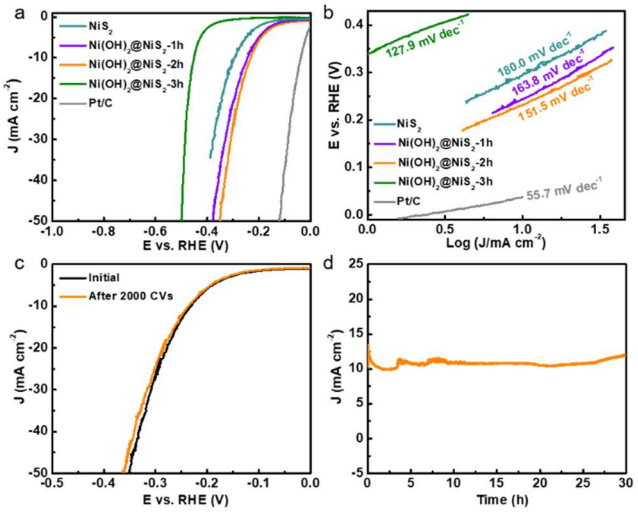

Figure 6. (a) LSV curves of all synthesized samples. (b) Tafel slopes, (c) LSV plots of $Ni(OH)_2$@NiS_2-2h before and after 2000 CVs. (d) The *i-t* curves of $Ni(OH)_2$@NiS_2-2h at 0.35 V vs. RHE.

The electrocatalytic HER performances of the yield samples were also evaluated in 1.0 M KOH. The related LSV plots in Figure 6a display an enhanced HER activity for $Ni(OH)_2$@NiS_2-2h sphere compared with the NiS_2 precursor. The needed overpotential at 10 mA cm^{-2} for $Ni(OH)_2$@NiS_2-2h is 233 mV, which has been dropped by 65 mV compared with the NiS_2 sample. The best HER activity for $Ni(OH)_2$@NiS_2-2h verifies that the moderately increasing $Ni(OH)_2$ is beneficial to HER thanks to the improved hydrophily and water dissociation ability of the $Ni(OH)_2$ species. We deduced that the excessive $Ni(OH)_2$ content may lead to the decrease of the conductivity of the catalyst. Table S2 shows that the HER activity is comparable with other reported catalysts. The fitted Tafel slope of $Ni(OH)_2$@NiS_2-2h is 151.5 mV dec^{-1}, smaller than the initial NiS_2 (180.0 mV dec^{-1}) (Figure 6b). This result reveals the HER kinetics has been accelerated by the construction of the $Ni(OH)_2$-NiS_2 interface. As discussed above, $Ni(OH)_2$ can be a preferable water cleavage compound due to its hydrophilicity. Furthermore, the stability was assessed by a fast CV scan and chronoamperometry. Encouragingly, the LSV of $Ni(OH)_2$@NiS_2-2h shows no previous degradation after the 2000 CV scan (Figure 6c). Moreover, it can stably operate for 30 h without noticeable fluctuation compared with Pt/C (Figure 6d, Figure S7b), which couples with the well-defined structure, further verifying the electrocatalytic stability of $Ni(OH)_2$@NiS_2-2h for HER.

CONCLUSION

In conclusion, we have synthesized a heterostructured $Ni(OH)_2$@NiS_2-2h hollow sphere acting as a promising bifunctional catalyst in alkaline electrolytes. The $Ni(OH)_2$ layer on the surface of NiS_2 exhibits three functions towards OER and HER. Specifically, $Ni(OH)_2$ can work as an active species for OER, while the NiS_2 expedited the electron transfer. Meanwhile, the spherical structure of NiS_2 enlarges the surface area for $Ni(OH)_2$ formation. In addition, for HER, the synergetic effect between $Ni(OH)_2$ and NiS_2 makes $Ni(OH)_2$@NiS_2-2h catalytically active for water cleavage and OH_{ad} desorption. As a result, the optimized $Ni(OH)_2$@NiS_2-2h displays improved catalytic performance for OER and HER compared to the pure NiS_2 sample. Besides, the $Ni(OH)_2$@NiS_2-2h resulted exhibits favorable stability for OER and HER. These results provide new insight into the design of bifunctional catalysts for electrochemical applications.

EXPERIMENTAL

Synthesis of NiS_2. NiS_2 was synthesized by a sample hydrothermal reaction. Briefly, $Ni(NO_3)_2{\cdot}6H_2O$ (0.291 g), urea (0.06 g) and L-cysteine (0.487 g) were dissolved in deionized water (50 mL) by ultrasonic treatment. Then, the above solution was transferred to a Teflon-lined autoclave and heated at 140 ℃ for 12 h. After cooling down to room temperature naturally, the black NiS_2 product was collected and rinsed with deionized water and ethyl alcohol three times and dried in a vacuum for later use.

Synthesis of $Ni(OH)_2$@NiS_2-*t*. Taking $Ni(OH)_2$@NiS_2-1h as an example, the above NiS_2 (0.05 g) was dissolved in a mixed solution of deionized water (20 mL) and absolute ethyl alcohol (50 mL) and refluxed at 85 ℃ for 1 h. After that, the powder was washed with ethyl alcohol several times and named $Ni(OH)_2$@NiS_2-1h.

Chin. J. Struct. Chem. **2022**, 41, 2208052-2208057
DOI: 10.14102/j.cnki.0254-5861.2022-0143

Similarly, $Ni(OH)_2$@NiS_2-2h and $Ni(OH)_2$@NiS_2-3h were obtained by changing the reflux time to 2 and 3 h, respectively.

■ ACKNOWLEDGEMENTS

This work is financially supported by the National Natural Science Foundation of China (52174283).

■ AUTHOR INFORMATION

Corresponding authors. Emails: 18905469551@163.com (S.J. Xu) and dongbin@upc.edu.cn (B. Dong)

■ COMPETING INTERESTS

The authors declare no competing interests.

■ ADDITIONAL INFORMATION

Supplementary information is available for this paper at http://manu30.magtech.com.cn/jghx/EN/10.14102/j.cnki.0254-5861.2022-0143

For submission: https://mc03.manuscriptcentral.com/cjsc

■ REFERENCES

(1) Cao, X.; Zhao, L.; Wulan, B.; Tan, D.; Chen, Q.; Ma, J.; Zhang, J. Atomic bridging structure of nickel-nitrogen-carbon for highly efficient electrocatalytic reduction of CO_2. *Angew. Chem. Int. Ed.* **2022**, 61, e202113918022.

(2) Li, M.; Feng, L. $NiSe_2$-CoS_2 with a hybrid nanorods and nanoparticles structure for efficient oxygen evolution reaction. *Chin. J. Struct. Chem.* **2022**, 41, 2201019-2201024.

(3) Guo, K.; Wang, Y.; Huang, J.; Lu, M.; Li, H.; Peng, Y.; Xi, P.; Zhang, H.; Huang, J.; Lu, S.; Xu, C. In situ activated $Co_{3-x}Ni_xO_4$ as a highly active and ultrastable electrocatalyst for hydrogen generation. *ACS Catal.* **2021**, 11, 8174-8182.

(4) Liu, Z.; Zhang, C.; Liu, H.; Feng, L. Efficient synergism of $NiSe_2$ nanoparticle/NiO nanosheet for energy-relevant water and urea electrocatalysis. *Appl. Catal. B Environ.* **2020**, 276, 119165.

(5) Dong, B.; Xie, J. Y.; Wang, N.; Gao, W. K.; Ma, Y.; Chen, T. S.; Yan, X. T.; Li, Q. Z.; Zhou, Y. L.; Chai, Y. M. Zinc ion induced three-dimensional Co_9S_8 nano-neuron network for efficient hydrogen evolution. *Renew. Energy* **2020**, 157, 415-423.

(6) Niu, C.; Zhang, Y.; Dong, J.; Yuan, R.; Kou, W.; Xu, L. 3D ordered macro-/mesoporous Ni_xCo_{100-x} alloys as high-performance bifunctional electrocatalysts for overall water splitting. *Chin. Chem. Lett.* **2021**, 32, 2484-2488.

(7) Yang, Y.; Yu, Y.; Li, J.; Chen, Q.; Du, Y.; Rao, P.; Li, R.; Jia, C.; Kang, Z.; Deng, P.; Shen, Y.; Tian, X. Engineering ruthenium-based electrocatalysts for effective hydrogen evolution reaction. *Nano-Micro Lett.* **2021**, 13, 160.

(8) Li, X. P.; Huang, C.; Han, W. K.; Ouyang, T.; Liu, Z. Q. Transition metal-based electrocatalysts for overall water splitting. *Chin. Chem. Lett.* **2021**, 32, 2597-2616.

(9) Liang, Z.; Yang, C.; Zhang, W.; Zheng, H.; Cao, R. Anion engineering of hierarchical Co-A (A = O, Se, P) hexagrams for efficient electrocatalytic oxygen evolution reaction. *Chin. Chem. Lett.* **2021**, 32, 3241-3244.

(10) Wang, Y.; Huang, J.; Wang, L.; She, H.; Wang, Q. Research progress of ferrite materials for photoelectrochemical water splitting. *Chin. J. Struct. Chem.* **2022**, 41, 2201054-2201068.

(11) Yao, Y. H.; Zhang, Z. Y.; Jiao, L. F. Development strategies in transition metal borides for electrochemical water splitting. *Energy Environ. Mater.* **2022**, 5, 470-485.

(12) Guo, F.; Wu, Y.; Chen, H.; Liu, Y.; Yang, L.; Ai, X.; Zou, X. High-performance oxygen evolution electrocatalysis by boronized metal sheets with self-functionalized surfaces. *Energy Environ. Sci.* **2019**, 12, 684-692.

(13) Gao, S.; Chen, H.; Liu, Y.; Gao, R.; Li, G. D.; Zou, X. Surface-clean, phase-pure multi-metallic carbides for efficient electrocatalytic hydrogen evolution reaction. *Inorg. Chem. Front.* **2019**, 6, 940-947.

(14) Li, P.; Hong, W.; Liu, W. Fabrication of large scale self-supported WC/$Ni(OH)_2$ electrode for high-current-density hydrogen evolution. *Chin. J. Struct. Chem.* **2021**, 40, 1365-1371.

(15) Fan, R. Y.; Xie, J. Y.; Liu, H. J.; Wang, H. Y.; Li, M. X.; Yu, N.; Luan, R. N.; Chai, Y. M.; Dong, B. Directional regulating dynamic equilibrium to continuously update electrocatalytic interface for oxygen evolution reaction. *Chem. Eng. J.* **2022**, 431, 134040.

(16) Wang, Y.; Chen, S.; Zhao, S.; Chen, Q.; Zhang, J. Interfacial coordination assembly of tannic acid with metal ions on three-dimensional nickel hydroxide nanowalls for efficient water splitting. *J. Mater. Chem. A* **2020**, 8, 15845-15852.

(17) Fu, C.; Wang, Y.; Huang, J. Hybrid of quaternary layered double hydroxides and carbon nanotubes for oxygen evolution reaction. *Chin. J. Struct. Chem.* **2020**, 39, 1807-1816.

(18) Xie, J. Y.; Fan, R. Y.; Fu, J. Y.; Zhou, Y. N.; Li, M. X.; Liu, H. J.; Ma, Y.; Wang, F. L.; Chai, Y. M.; Dong, B. Double doping of V and F on Co_3O_4 nanoneedles as efficient electrocatalyst for oxygen evolution. *Inter. J. Hydrogen Energy* **2021**, 46, 19962-19970.

(19) Du, J.; Li, F.; Sun, C. L. Metal-organic frameworks and their derivatives as electrocatalysts for the oxygen evolution reaction. *Chem. Soc. Rev.* **2021**, 50, 2663-2695.

(20) Wang, Y.; Ma, J.; Wang, J.; Chen, S.; Wang, H.; Zhang, J. Interfacial scaffolding preparation of hierarchical PBA-based derivative electrocatalysts for efficient water splitting. *Adv. Energy Mater.* **2019**, 9, 1802939.

(21) Fan, R. Y.; Zhou, Y. N.; Li, M. X.; Xie, J. Y.; Yu, W. L.; Chi, J. Q.; Wang, L.; Yu, J. F.; Chai, Y. M.; Dong, B. In situ construction of Fe(Co)OOH through ultra-fast electrochemical activation as real catalytic species for enhanced water oxidation. *Chem. Eng. J.* **2021**, 426, 131943.

(22) Zhou, Y. N.; Wang, F. L.; Dou, S. Y.; Shi, Z. N.; Dong, B.; Yu, W. L.; Zhao, H. Y.; Wang, F. G.; Yu, J. F.; Chai, Y. M. Motivating high-valence Nb doping by fast molten salt method for NiFe hydroxides toward efficient oxygen evolution reaction. *Chem. Eng. J.* **2022**, 427, 131643.

(23) Wei, C.; Sun, Y.; Scherer, G. G.; Fisher, A. C.; Scherburne, M.; Ager, J. W.; Xu, Z. J. Surface composition dependent ligand effect in tuning the activity of nickel-copper bimetallic electrocatalysts toward hydrogen evolution in alkaline. *J. Am. Chem. Soc.* **2020**, 142, 7765-7775.

(24) Zhang, P.; Lu, X. F.; Nai, J. W.; Zang, S. Q.; Lou, X. W. Construction of hierarchical Co-Fe oxyphosphide microtubes for electrocatalytic overall water splitting. *Adv. Sci.* **2019**, 6, 1900576.

(25) McCrum, I. T.; Koper, M. T. M. The role of adsorbed hydroxide in hydrogen evolution reaction kinetics on modified platinum. *Nat. Energy* **2020**, 5, 891-899.

(26) Zheng, M.; Guo, K.; Jiang, W. J.; Tang, T.; Wang, X.; Zhou, P.; Du, J.; Zhao, Y.; Xu, C.; Hu, J. S. When MoS_2 meets FeOOH: a "one-stone-two-birds" heterostructure as a bifunctional electrocatalyst for efficient alkaline water splitting. *Appl. Catal. B Environ.* **2019**, 244, 1004-1012.

(27) Lv, C. C.; Wang, X. B.; Gao, L. J.; Wang, A. J.; Wang, S. F.; Wang, R. N.; Ning, X. K.; Li, Y. G.; Boukhvalov, D. W.; Huang, Z. P.; Zhang, C. Triple

DOI: 10.14102/j.cnki.0254-5861.2022-0143

functions of $Ni(OH)_2$ on the surface of WN nanowires remarkably promoting electrocatalytic activity in full water splitting. *ACS Catal*. **2020**, 10, 13323-13333.

(28) Subbaraman, R.; Tripkovic, D.; Strmcnik, D.; Chang, K. C.; Uchimura, M.; Paulikas, A. P.; Stamenkovic, V.; Markovic, N. M. Enhancing hydrogen evolution activity in water splitting by tailoring Li^+-$Ni(OH)_2$-Pt interfaces. *Science* **2011**, 334, 1256-1260.

(29) Xu, Q. C.; Jiang, H.; Zhang, H. X.; Hu, Y. J.; Li, C. Z. Heterogeneous interface engineered atomic configuration on ultrathin $Ni(OH)_2/Ni_3S_2$ nanoforests for efficient water splitting. *Appl. Catal. B Environ*. **2019**, 242, 60-66.

(30) Wei, Y.; Zhang, X.; Wang, Z.; Yin, J.; Huang, J.; Zhao, G.; Xu, X. Metal-organic framework derived NiCoP hollow polyhedrons electrocatalyst for pH-universal hydrogen evolution reaction. *Chin. Chem. Lett*. **2021**, 32, 119-124.

(31) Zheng, Y.; Jiao, Y.; Zhu, Y.; Li, L. H.; Han, Y.; Chen, Y.; Jaroniec, M.; Qiao, S.-Z. High electrocatalytic hydrogen evolution activity of an anomalous ruthenium catalyst. *J. Am. Chem. Soc*. **2016**, 138, 16174-16181.

(32) Ma, Q. Y.; Hu, C. Y.; Liu, K. L.; Hung, S.-F.; Ou, D. H.; Chen, H. M.; Fu, G.; Zheng, N. F. Identifying the electrocatalytic sites of nickel disulfide in alkaline hydrogen evolution reaction. *Nano Energy* **2017**, 41, 148-153.

(33) Kuang, P. Y.; He, M.; Zou, H. Y.; Yu, J. G. 0D/3D MoS_2-NiS_2/N-doped graphene foam composite for efficient overall water splitting. *Appl. Catal. B: Environ*. **2019**, 254, 15-25.

(34) Kuang, P. Y.; Wang, Y. R.; Zhu, B. C.; Xia, F. J.; Tung, C. W.; Wu, J. S.; Chen, H. M. Pt Single atoms supported on N-doped mesoporous hollow carbon spheres with enhanced electrocatalytic H_2-evolution activity. *Adv. Mater.* **2021**, 33, 2008599.

(35) Chang, K.; Chen, W. X. l-Cysteine-assisted synthesis of layered MoS_2/graphene composites with excellent electrochemical performances for lithium ion batteries. *ACS Nano*. **2011**, 5, 4720.

(36) Zeng, L. Y.; Sun, K.; Chen, Y. J.; Liu, Z.; Chen, Y. J.; Pan, Y.; Zhao, R. Y.; Liu, Y. Q.; Liu, C. G. Neutral-pH overall water splitting catalyzed efficiently by a hollow and porous structured ternary nickel sulfoselenide electrocatalyst. *J. Mater. Chem. A* **2019**, 7, 16793.

(37) Peng, S.; Li, L.; Tan, H.; Cai, R.; Shi, W.; Li, C.; Mhaisalkar, S. G.; Srinivasan, M.; Ramakrishna, S.; Yan, Q. MS_2 (M = Co and Ni) hollow spheres with tunable interiors for high-performance supercapacitors and photovoltaics. *Adv. Funct. Mater*. **2014**, 24, 2155-2162.

(38) Guo, Z.; Wang, X. Atomic layer deposition of the metal pyrites FeS_2, CoS_2, and NiS_2. *Angew. Chem. Int. Ed*. **2018**, 57, 5898-5902.

(39) Zhu, Y.; Chen, G.; Zhong, Y.; Zhou, W.; Shao, Z. Rationally designed hierarchically structured tungsten nitride and nitrogen-rich graphene-like carbon nanocomposite as efficient hydrogen evolution electrocatalyst. *Adv. Sci*. **2018**, 5, 1700603.

(40) Fu, Z. W.; Hu, J. T.; Hu, W. L.; Yang, S. Y.; Luo, Y. F. Quantitative analysis of Ni^{2+}/Ni^{3+} in $Li(Ni_xMn_yCo_z)O_2$ cathode materials: non-linear least-squares fitting of XPS spectra. *Appl. Surf. Sci.* **2018**, 441, 1048-1056.

(41) Gao, M. R.; Liang, J. X.; Zheng, Y. R.; Xu, Y. F.; Jiang, J.; Gao, Q.; Li, J.; Yu, S. H. An efficient molybdenum disulfide/cobalt diselenide hybrid catalyst for electrochemical hydrogen generation. *Nat. Commun*. **2015**, 6, 5982.

(42) Ou, G.; Xu, Y. S.; Wen, B.; Lin, R.; Ge, B. G.; Tang, Y.; Liang, Y. W.; Yang, C.; Huang, K.; Zu, D.; Yu, R.; Chen, W. X.; Li, J.; Wu, H.; Liu, L. M.; Li, Y. D. Tuning defects in oxides at room temperature by lithium reduction. *Nat. Commun.* **2018**, 9, 1302.

(43) Hu, W. B.; Liu, Y.; Withers, R. L.; Frankcombe, T. J.; Norén, L.; Snashall, A.; Kitchin, M.; Smith, P.; Gong, B.; Chen, H.; Schiemer, J.; Brink, F.; Jennifer, W. L. Electron-pinned defect-dipoles for high-performance colossal permittivity materials. *Nat. Mater.* **2013**, 12, 821-826.

(44) Xiao, Z. H.; Huang, Y. C.; Dong, C. L.; Xie, C.; Liu, Z. J.; Du, S. Q.; Chen, W.; Yan, D. F.; Tao, L.; Shu, Z. W.; Zhang, G. H.; Duan, H. G.; Wang, Y. Y.; Zou, Y. Q.; Chen, R.; Wang, S. Y. Operando identification of the dynamic behavior of oxygen vacancy-rich Co_3O_4 for oxygen evolution reaction. *J. Am. Chem. Soc*. **2020**, 142, 12087-12095.

(45) Zhu, Y. M.; Zhang, L.; Zhao, B.; Chen, H. J.; Liu, X.; Zhao, R.; Wang, X. W.; Liu, J.; Chen, Y.; Liu, M. L. Improving the activity for oxygen evolution reaction by tailoring oxygen defects in double perovskite oxides. *Adv. Funct. Mater*. **2019**, 29, 1901783.

(46) Zeng, Y.; Cao, Z.; Liao, J.; Liang, H.; Wei, B.; Xu, X.; Xu, H.; Zheng, J.; Zhu, W.; Cavallo, L.; Wang, Z. Construction of hydroxide PN junction for water splitting electrocatalysis. *Appl. Catal. B: Environ*. **2021**, 292, 120160.

(47) Yuan, M. L.; Chen, J. W.; Bai, Y. L.; Liu, Z. J.; Zhang, J. X.; Zhao, T. K.; Shi, Q. N.; Li, S. W.; Wang, X.; Zhang, G. J. Electrochemical C-N coupling with perovskite hybrids toward efficient urea synthesis. *Chem. Sci*. **2021**, 12, 6048-6058.

(48) Liu, Y. P.; Liang, X.; Gu, L.; Zhang, Y.; Li, G. D.; Zou, X. X.; Chen, J. S. Corrosion engineering towards efficient oxygen evolution electrodes with stable catalytic activity for over 6000 hours. *Nat. Commun.* **2018**, 9, 2609.

(49) Kim, D.; Park, J.; Lee, J.; Zhang, Z.; Yong, K. $Ni(OH)_2$-WP hybrid nanorod arrays for highly efficient and durable hydrogen evolution reactions in alkaline media. *ChemSusChem*. **2018**, 11, 3618-3624.

Received: May 28, 2022
Accepted: June 18, 2022
Published online: June 28, 2022
Published: July 25, 2022

DOI: 10.14102/j.cnki.0254-5861.2022-0143